Advanced Physics Lab II

Lab Report #4

Zeeman Effect

Group 1
Noah Horne, Luka Burduli

31/03/2025

Dr. Arnulf Materny
Dr. Faezeh Mohaghegh

We hereby declare that we (Luka Burduli and Noah Horne) are the sole authors of this lab report and have not used any sources other than those listed in the bibliography and identified as references throughout the report.

_____ _____

Contents

1 Abstract

The normal Zeeman effect refers to a fundamental quantum phenomenon exhibited by atomic systems subject to an external magnetic field which have a net spin of 0. Specifically, the Zeeman effect gives rise to the lifting of degeneracy on the quantized energy levels of a nucleus, giving rise to the magnetic moment quantum number M_j, the cornerstone of this removed degeneracy. By analyzing the changes in wavenumber $\Delta\tilde{\nu}$ corresponding to different quantum energy transitions–governed by the selection rules $\Delta M_j = -1, 0, 1$–one can accurately determine the Bohr magneton, an important proportionality constant relating the energy levels of a nucleus and the magnitude of an external magnetic field. Through the help of a measured relationship between the current across electromagnetic coils and their corresponding magnetic flux density at the location of a Cadmium lamp given by the equation:

$$B = 0.0585(I) + 3.66 \cdot 10^{-3} \tag{1.1}$$

a value of the Bohr magneton μ_B was calculated very accurate to the theoretical value $\approx 9.27 \cdot 10^{-24}[JT^{-1}]$ using the relationship of change in wavenumber $\Delta\tilde{\nu}$ and magnetic flux density B:

$$\mu_B = (9.30 \pm 0.31) \cdot 10^{-24}[JT^{-1}] \tag{1.2}$$

As one can observe, the value of the Bohr magneton μ_B calculated adheres very closely to the theoretical value. After this calculation, a qualitative analysis of the longitudinal Zeeman effect was performed successfully. All results obtained in this investigation adhere to the theoretical expectations to a considerable degree.

2 Introduction & Theory

This investigation serves as a quantitative and qualitative analysis of the transverse and longitudinal normal Zeeman Effect on the red spectral line (643.8 [nm]) of Cadmium. Throughout the course of this investigation, the relationship between the magnetic field strength B across a Cadmium Lamp (Cd) and change in wavenumber $\Delta\tilde{\nu}$ is measured and consequently applied to the accurate calculation of the Bohr Magneton μ_B. To observe the small difference in wavelength caused by such Zeeman Effect-induced splitting, a Fabry-Perot Etalon is used, capable of detecting changes in wavelength up to 0.002 [nm] (Materny & Mohaghegh, 2025). A Fabry Perot etalon functions as an optical interferometer consisting of two diametrically opposed mirrors where light can only pass through if resonance is achieved. When constructive interference occurs, a bright central maxima is observed on the interference pattern on a screen. By analyzing the radius of these peaks, the exact wavelengths of the spectral lines and their corresponding shifts due to the Zeeman effect can be determined.

When the nucleus of an atom is excited it emits photons based on transitions between its atomic energy levels. It is known that these atomic energy levels are discretized with respect to very specific frequency ranges dependent on the configuration of their electron shells, sub-shells, and total angular momentum. In atomic systems which do not contain an external magnetic flux density B, the states of electrons in their respective orbitals are degenerate, each degenerate state sharing the same angular momentum $\vec{J}$. When the atom is placed into a (weak to avoid the Paschen-Back effect) magnetic field $\vec{B}$ however, such degeneracy of the states is lifted, leading to the splitting of singlets into Lorentz Triplets due to the now additional spin microstate configurations $|\uparrow\downarrow\rangle, |00\rangle, |\downarrow\uparrow\rangle$. When subject to an orthogonal external magnetic field, the discretization of the energy levels in the nucleus can be described by the formula:

$$E = g_j \mu_B M_j B_0, \quad M_j = -j, -j+1, \ldots, j-1, j \tag{2.1}$$

where g_j is the Landé g-factor of the atomic system, μ_B is the Bohr Magneton ($\approx 9.274 \cdot 10^{-24}$ $[JT^{-1}]$), M_j is the magnetic moment quantum number, and B_0 is the magnitude of the magnetic field. This theoretical discretization is a direct result of the quantization of the eigenvalues of the magnetic moment operator $\vec{\mu}$ on the magnetic field $\vec{B}$, specifically in its z component. From this equation alone (2.1), it is reasonable to postulate a linear relationship between the magnitude of the magnetic field strength and the change in wavenumber $\Delta\nu$ of the Cadmium (Cd) emitted photons. To investigate this discretization further in the context of the specific investigation, the red spectral line of the Cadmium system corresponds to the shift in angular quantum number j from $j = 2 \rightarrow 1$–corresponding to a transition from the $1D_2$ sub-shell to the $1P_1$ sub-shell (Fernandez, SepÃžlveda, Trincavelli, & Castellano, 2022).

When $j = 2$, M_j has 5 possible states, $M_2 = -2, -1, 0, 1, 2$ and when $j = 1$, $M_j = -1, 0, 1$. Consequently, 9 possible transitions are allowed, corresponding the 3 different energy levels. These 3 energy levels correspond to the selection rules $\Delta M_j = 0, \pm 1$. For $\Delta M_j = 0$, the emitted photons are emergent parallel polarized to the direction of the magnetic field vector, and hence labeled to be part of the π-line. For changes in magnetic moment quantum number $\Delta M_j = \pm 1$, the photons emerge vertically polarized to the magnetic field, labeled as the σ_+ and σ_- spectral lines respectively. This experiment only focuses on the difference in wavenumber of the $\sigma_\pm$ lines, which are separated through an intermediary analyzer lens to remove the parallel polarized central π-line. To better visualize these split spectral lines, a Fabry-Perot Interferometer is used to extract the corresponding frequency shifts due to the Zeeman effect visualized by a circular ring interference pattern. By analyzing the relationship between the magnetic field strength across the Cadmium Lamp and the differences in radii of these p order $\sigma_\pm$ split interference rings $r_{p,a}$,$r_{p,b}$, $r_{p+1,a}$,$r_{p+1,b}$, the corresponding difference in wavenumbers $\Delta\tilde{\nu}$ can be found, and the Bohr Magneton μ_B calculated.

To calculate this aforementioned difference in wavenumber $\Delta\tilde{\nu}$, one makes use of two important quantities related to the difference of interference pattern radii: Δ and δ, given below.

$$\Delta = \frac{1}{4}\sum_{p=1}^{2}\left(\Delta_a^{2p,2p-1} + \Delta_b^{2p,2p-1}\right) \tag{2.2}$$

$$\delta = \frac{1}{4}\sum_{p=1}^{4}\delta_{a,b}^{p} \tag{2.3}$$

These mean difference factors Δ and δ are calculated as the average of the shift specific difference factors $\Delta_a^{p+1,p}, \Delta_b^{p+1,p}, \delta_{a,b}^{p}$, which describe the difference of squares of the different interference ring radii, defined as follows:

$$\Delta_a^{p+1,p} = r_{p+1,a}^2 - r_{p,a}^2 = \frac{2f^2}{n_{0,a}} \approx \frac{2f^2}{n_{0,b}} = r_{p+1,b}^2 - r_{p,b}^2 = \Delta_b^{p+1,p} \tag{2.4}$$

where $r_{p,a}, r_{p+1,a}$ describes the radius at the pth and $(p+1)$th order interference ring corresponding to the σ_--line, and $r_{p,b}, r_{p+1,b}$ corresponds to the σ_+-line. Similarly, $\delta_{a,b}^{p}$ is defined as the difference of squares of the radii for the $\sigma_\pm$ lines on the same angular momentum quantum ring:

$$\delta_{a,b}^{p} = r_{p,a}^2 - r_{p,b}^2 \tag{2.5}$$

The equation 2.5, when averaged, yields an important quantity proportional to the square of the frequency shift due to Zeeman splitting. Taking the ratio of the two mean difference factors Δ and δ, one achieves an expression proportional to the shift in wavenumber $\Delta\tilde{\nu}$:

$$\Delta\tilde{\nu} = \frac{1}{2t}\frac{\delta}{\Delta} \tag{2.6}$$

where t is the spacing between the mirrors used in the Fabry-Perot etalon/interferometer (3 mm) (Materny & Mohaghegh, 2025). As is, equations 2.2-2.6 allow a thorough examination into the relationship between magnetic field strength and change in wavenumber. To extract the Bohr-Magneton μ_B, from such a proportional relationship, it is possible to relate the shift in wavenumber directly to the Bohr magneton μ_B through the formula:

$$\mu_B = hc\frac{\Delta\tilde{\nu}}{2B} \tag{2.7}$$

Equation 2.7 is derived from the equivalence of the shift in energy ΔE to the magnitude of the magnetic field B and the difference in wavenumbers in one of the σ spectral lines, e.g.

$$\Delta E = hc\frac{\Delta\tilde{\nu}}{2} = \mu_B B \tag{2.8}$$

By direct application of equation 2.7, one can calculate the Bohr magneton μ_B by determining the change in wavenumber $\Delta\tilde{\nu}$ between the two σ split spectral lines of the Cadmium triplet and the mean difference factors Δ and δ obtained through an average of the squared differences of radii observed in the interference pattern of the Fabry-Perot interferometer. While the transverse normal Zeeman effect is the primary subject of this investigation (normal due to the absence of net electron spin $\sum \vec{S}_i = 0$), it is crucial to acknowledge the longitudinal normal Zeeman effect as well. When photons are emitted parallel to the direction vector of the magnetic field $\vec{B}$, they emerge circularly polarized to the left and right, corresponding to σ_+ and σ_- spectral lines respectively (Materny & Mohaghegh, 2025). To observe that these electromagnetic waves are indeed polarized, one makes use of a birefringent $\lambda/4$ plate to turn the circularly polarized waves into orthogonal linearly polarized waves which can be separated through the use of an analyzer. As this effect exhibits primarily qualitative effects, these results were only demonstrated visually and no numerical measurements were taken.

3 Setup & Experimental Procedure

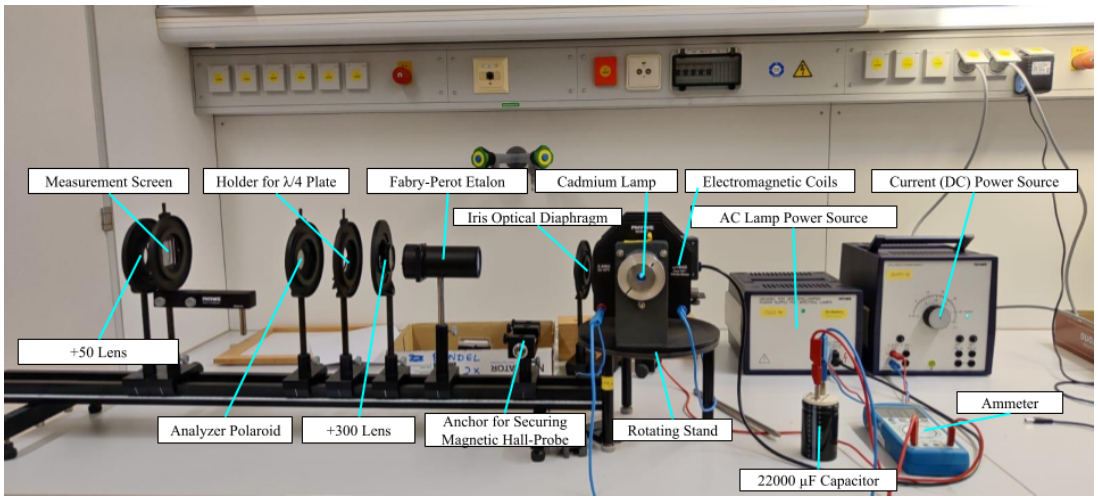

Figure 1: Annotated Setup of Transverse Normal Zeeman Effect Investigation

To accurately determine the relationship between the magnetic flux density across the Cadmium lamp and the corresponding change in wavenumber of the $\sigma_\pm$ spectral lines, the relationship between current across the electromagnetic coils and magnetic flux density is measured. To do so, the optical bench is first aligned using a spirit level, allowing the electromagnetic coils to be properly oriented along the bench. Measurements of the magnetic flux density were conducted for electromagnetic coil currents I ranging from 1.1 [A] to 10.07 [A]. The respective values were tabulated and a linear plot constructed. Through the interpolation of these data points, accurate values of the magnetic flux density B with respect to current I can later be computed formulaically by the trend line of the relationship.

After a B-I relationship is constructed, the current is fixed starting at $4[A]$, and the optical setup adjusted such that at least 4 interference rings can be seen on the measurement screen through the +50 objective lens. Once these rings are sharp and visible and the splitting is clearly evident on the screen, the origin of the measurement scale is aligned to lie at the center of the interference pattern. It is important to note that while this process was performed as accurately as possible, no clear markings are present at the center of the interference pattern, so a small systematic error could be introduced during this step. After this calibration procedure was complete, the radii of the σ_+ and σ_- lines were measured for diffraction order $1, 2, 3$ and 4 respectively. Using these radii, the corresponding specific difference factors $\delta^p_{a,b}$ and $\Delta^{p+1,p}_a, \Delta^{p+1,p}_b$ were calculated using formulas 2.4 and 2.5, and the mean difference terms δ and Δ computed. After all measurements for the radii were taken, the current is increased by 1[A], and the same measurements are taken until the current across the electromagnetic coils reaches 8[A]. Using the calculated values of δ and Δ, the change in wavenumber $\Delta\tilde{\nu}$ and magnetic flux density B is calculated for each current, using formula 2.6 and the trend line of the B-I relationship. By extracting the slope of the graph of change in wavenumber against magnetic flux density, one consequently computes the value of the Bohr Magneton μ_B by applying equation 2.7.

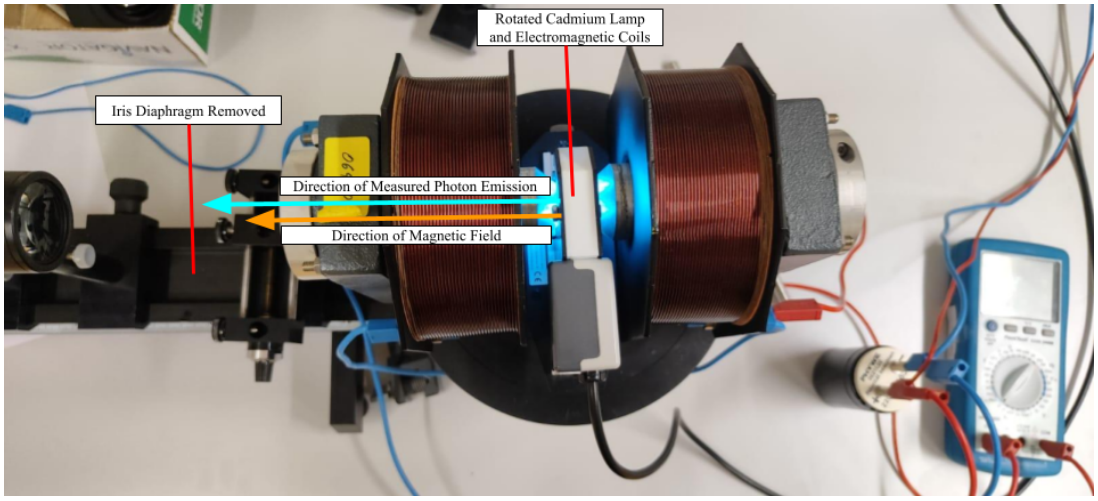

Figure 2: Annotated Setup for Longitudinal Zeeman Effect Investigation

The last aspect of the investigation features a qualitative analysis of the longitudinal normal Zeeman effect. According to the afore-established theory, electromagnetic waves emergent parallel to the external B-field become left and right circularly polarized according to the σ_+ and σ_- spectral lines. To revert this polarization to two orthogonal linear polarizations, a $\lambda/4$ plate is used. As a result, the σ_- and σ_+ polarizations are separated by positioning the analyzer at angles of $+45°$ and $-45°$ respectively such that each line can be observed individually.

4 Results and Data Analysis

The first aspect of the investigation of the Zeeman effect involves the construction of an interpolatory trend between the current across the electromagnetic coils, and the magnetic flux density across the Cadmium lamp. To establish such a directly proportional relationship, the current was increased gradually such that 10 different data points and their corresponding magnetic flux densities B were measured. This data allowed the determination of the magnetic flux density of specific current I values during later stages of the investigation where a measure of the flux density was critical–e.g. in the calculation of the Bohr Magneton using equation 2.7. To do so, the optical diaphragm and Cadmium lamp were removed from between the electromagnetic coils and replaced with a Hall magnetic flux probe. To ensure optimal measurements, the probe was aligned in such a way that a maximum magnetic flux density was observed. After the calibration procedure was complete, measurements were then taken to determine the precise relationship of the magnetic flux density B and the current I. The resultant raw data tables for the magnetic flux density against electromagnetic coil current can be seen in the appendix of this report. For clarity and for basis of commentary, the plot of the data is given below.

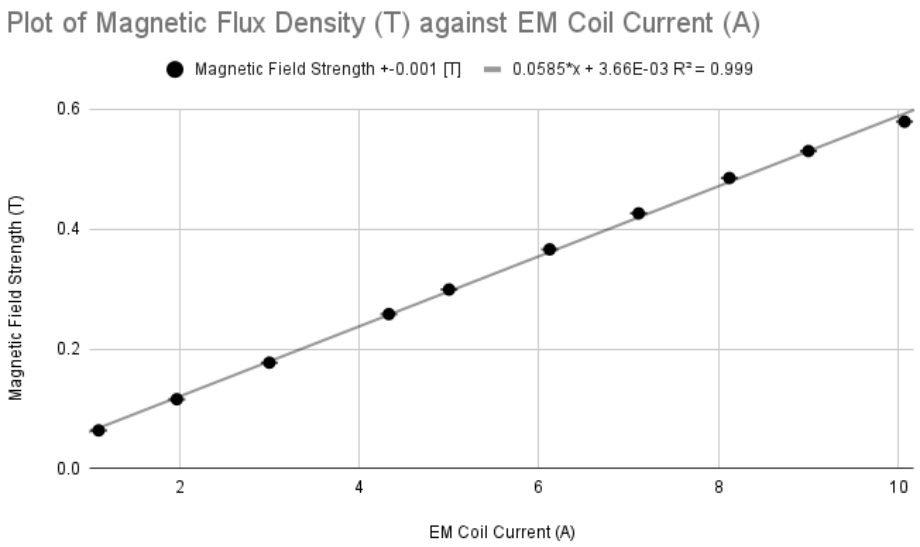

Figure 3: Plot of Magnetic Flux Density (T) against EM Coil Current (A)

The trend line of the plot above clearly demonstrates a positive linear dependence between the current I and magnetic flux density B. It is important to note as well that the error bars are indeed included for this graph, however so small in comparison that they are nearly non-visible. From this graph, the following equation was obtained with an absolute error of the slope of $\pm 7.03 \cdot 10^{-4}[TA^{-1}]$ and correlation coefficient $R^2 = 0.999$:

$$B = 0.0585(I) + 3.66 \cdot 10^{-3} \tag{4.1}$$

After this measurement series was complete and the equation relationship determined, the Fabry-Perot interferometer was aligned perpendicular to the emission direction of the Cadmium lamp, now placed between the electromagnetic coils at a location of maximum magnetic flux density. As the magnetic field was applied, the $(643.8[nm])$ spectral line was split into multiple components corresponding to the fringe pattern of the etalon splitting from discrete singular radii to two rings separate rings per diffraction order, each visualizing a corresponding σ_- and σ_+ line respectively. The radii of each p-th order diffraction ring $r_{p,b}$ and $r_{p,b}$ of the split components were measured, where a and b refer to the σ_- and σ_+ lines respectively. To ensure the clarity and concision of this report, a sample investigation for a single fixed current value is given, rather than all 5 currents. The resultant data table for a current of $8[A]$ corresponding to a magnetic flux density $B = 0.4714 \pm (0.7 \cdot 10^{-3})$ [T] is given below.

Table 1: Measured Ring Radii [mm] and calculated $\Delta_a, \Delta_b, \delta$ for current $8[A] \rightsquigarrow 0.4714[T]$

Diff. Order P	$r_{p,a} \pm 0.05[mm]$	$r_{p,b} \pm 0.05[mm]$	δ	Δ_a	Δ_b
1	4.8	4	7.04		
2	7	6.4	8.04	25.96	24.96
3	8.6	8.3	5.07		
4	10.1	9.6	9.85	28.05	23.27

As one can observe from table 1, the separation radii stays relatively similar despite change in diffraction order. Applying formulas 2.3 and 2.2 and taking an average of the δ's in the above table, the mean difference factors δ and Δ for a magnetic flux density of $0.4714[T]$ were obtained as:

$$\delta_{8A} = 7.50 \pm 0.99[m^2] \tag{4.2}$$

$$\Delta_{8A} = 25.56 \pm 0.99[m^2] \tag{4.3}$$

Furthermore, as these two difference factors are formulaically related to the change in wavenumber of the Cadmium system through their ratio, one may apply formula 2.6 to calculate this corresponding shift $\Delta\tilde{\nu}$. Upon substitution, $\Delta\tilde{\nu}$ was calculated to be:

$$\Delta\tilde{\nu}_{8A} = 48.90 \pm 6.77[m^{-1}] \tag{4.4}$$

With these measurements taken, the exact same procedure was repeated, and the wavenumber calculated for currents of $7[A], 6[A], 5[A]$ and $4[A]$–corresponding to magnetic flux densities $0.413[T], 0.354[T], 0.296[T]$ and $0.238[T]$. The resultant raw data tables and computations of the difference factors for each magnetic flux density is tabulated in the appendix of this report. Once all changes in wavenumber $\Delta\tilde{\nu}$ were calculated, their relationship with the magnetic flux density across the Cadmium lamp was examined. The results of these calculations alongside their corresponding errors can be seen in the table below:

Table 2: Change in Wavenumber $\Delta\tilde{\nu}$ against Magnetic Flux Density (T)

Current $\pm 0.01[A]$	Magnetic Flux Density [T]	Error of the Magnetic Flux Density [mT]	$\Delta\tilde{\nu}$ $[m^{-1}]$	Error of $\Delta\tilde{\nu}$ $[m^{-1}]$
8.00	0.471	5.62	48.90	6.78
7.00	0.413	4.92	43.87	3.94
6.00	0.354	4.22	37.40	3.37
5.00	0.296	3.52	33.22	5.53
4.00	0.238	2.81	26.89	1.72

Examining the tabulated data, it is already possible to observe a positive linear realtionship between the change in wavenumber and the magnetic flux density. As the change in wavenumber increases, it is also clear that it absolute error grows, seen in the rightmost column, likely due to the direct scaling of the absolute error with the magnetic flux density. After these computations were made and tabulated, the magnetic field strength B against change in wavenumber $\Delta\tilde{\nu}$ was plotted:

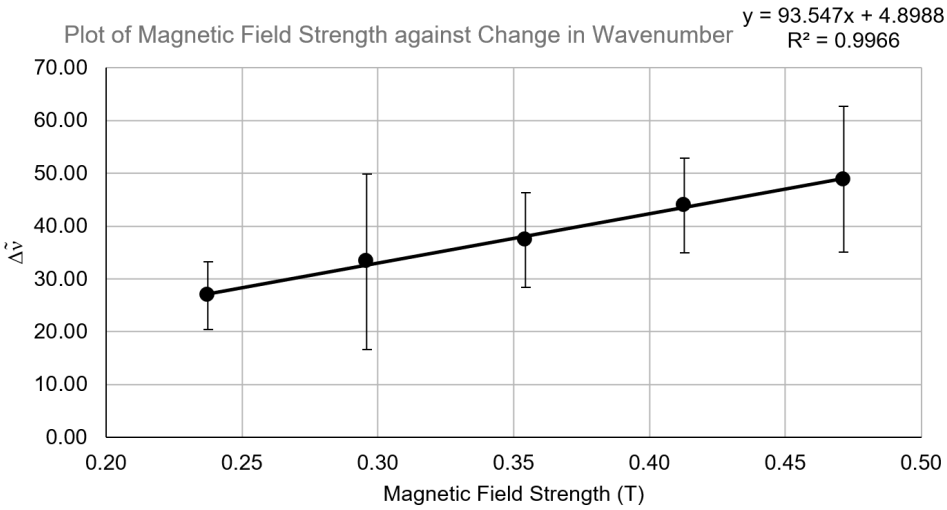

Figure 4: Plot of Change in Wavenumber $\Delta\tilde{\nu}$ against Magnetic Field Strength B

From the plot, a clearly strong linear relationship is observed with a slope of $93.55 \pm 3.14[m^{-1}T^{-1}]$ and correlation coefficient $R^2 = 0.9966$. Using the equation of the graph:

$$\Delta\tilde{\nu} = 93.547B + 4.8988 \tag{4.5}$$

one extracts the slope and consequently substitutes into equation 2.7 to determine an accurate estimate of the Bohr magneton μ_B which only deviates from the theoretical value by $\approx 3 \cdot 10^{-26}[JT^{-1}]$:

$$\mu_B = (9.30 \pm 0.31) \cdot 10^{-24}[JT^{-1}] \tag{4.6}$$

With the value of the Bohr magneton μ_B calculated with a commensurable uncertainty, the investigation of the transverse Zeeman effect was concluded. Transitioning to the final aspect of the investigation, the longitudinal Zeeman effect was qualitatively analyzed. To observe such a longitudinal Zeeman effect (see figure 5), the experimental setup was modified such that the optical path of the Cadmium light aligned parallel to the magnetic field. Due to this configuration, emitted $\sigma_{\pm}$ lines emerged circularly polarized to the left and right. As circularly polarized electromagnetic waves cannot be separated through the use of a linear analyzer polaroid, a quarter-wave plate was introduced in between to convert such circularly polarized light to two orthogonal linear beams. By following the $\lambda/4$ plate with a rotating linear analyzer polaroid, the angle could be changed, and the corresponding separate lines observed.

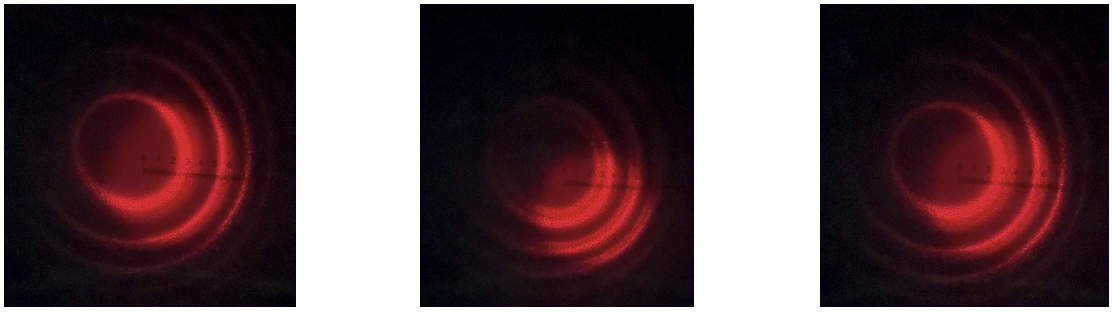

Analyzer at 45° Analyzer at 0° Analyzer at -45°

Figure 5: Analyzer at different angles

Observing the images above, it is clear that at an analyzer angle of $0°$, the transmitted light showed two distinct intensity peaks corresponding to the two circularly polarized components of the split spectral lines. This occurs as components from both left- and right-circularly polarized beams are still able to pass through. At $\pm 45°$, the intensity a single $\sigma_{\pm}$ beam reaches its maximum, indicated by the presence of a single brighter line visible at each diffraction order. Such behavior directly confirms that the light was indeed circularly polarized, as the linearly polarized emergent light from the quarter-wave plate was easily separated into individual $\sigma_{\pm}$ spectrum line components through the introduction of an analyzer.

5 Error Analysis

For all errors involving the slope of the graph, the uncertainty of the slope was approximated using the built-in function (LINEST), which works by approximating the linear slope of a set of data points through the least squares method. As a byproduct, the error of the slope is given in absolute form. Due to the efficiency of this method and the large quantity of graphs, it was the clear choice for this investigation. For all errors involving numerical calculations with propagated error, the root sum of squares method (RSS) was employed. This method involves calculating the propagated error of a formulaic value by computing all partial derivatives with respect to all error-prone parameters, and taking it under a square root: the formula given below.

$$\Delta y = \sqrt{\sum_{i=0}^{n} \left(\frac{\partial y}{\partial x_i} \cdot \Delta x_i \right)^2} = \sqrt{\left(\frac{\partial y}{\partial x_1} \cdot \Delta x_1 \right)^2 + \cdots + \left(\frac{\partial y}{\partial x_n} \cdot \Delta x_n \right)^2} \tag{5.1}$$

During the magnetic field's calibration phase, the Helmholtz coils' current was varied with a known instrumental uncertainty of $\Delta I = 0.01$. The corresponding magnetic field error was $\Delta B = 0.001T$. A linear regression of the calibration plot of the current against the magnetic field yielded the slope with uncertainty $\pm 7.03 \cdot 10^{-4} [AT^{-1}]$, with a strong correlation coefficient of $R^2 = 0.999$.

In the transverse Zeeman effect analysis, uncertainties in measuring the interference ring radii introduced error into the determination of both δ and Δ values. Here, an example for 8A is shown; the errors for the other currents were calculated using the same method. For a current of 8A and a corresponding B field B=0.4714T, the calculated values were $\Delta_{error}(\delta_{8A}) = \pm 0.997 [m^2]$ and $\Delta_{error}(\Delta_{8A}) = \pm 0.999 [m^2]$. The uncertainties were calculated using standard deviation over the square root of the number of measurements $(\sigma/\sqrt{n})$.

The uncertainty in the change in wavenumber $\Delta\tilde{\nu}$ was computed using error propagation from δ and Δ. t=3$[mm]$ the thickness of the etalon was assumed to have no uncertainty, as it was given from the literature (Materny & Mohaghegh, 2025). The corresponding propagated error of change in wavenumber $\Delta\tilde{\nu}$ is given by:

$$\Delta_{error}(\Delta\tilde{\nu}) = \sqrt{(\frac{\Delta_{error}(\delta_{8A})}{2t\Delta_{8A}})^2 + (\frac{\delta_{8A}\Delta_{error}(\Delta_{8A})}{2t\Delta_{8A}^2})^2} \tag{5.2}$$

$$= \sqrt{(\frac{0.997}{2 \cdot 0.003 \cdot 25.56})^2 + (\frac{7.5 \cdot 0.998}{2 \cdot 0.003 \cdot 25.56^2})^2} = 6.776 [m^{-1}]$$

To calculate the Bohr magneton μ_B, the linear relationship between $\Delta\tilde{\nu}$ and B was investigated. A linear regression yielded a slope of $m = 93.55 \pm 3.14 [m^1 T]$, where the error was calculated using the LINEST function. Using equation 2.7 the Bohr magneton was calculated, and the error for it was calculated using RSS error propagation as previously performed:

$$\Delta\mu_B = \frac{hc}{2} \cdot \Delta = (6.63 \cdot 10^{-34} \cdot 2.998 \cdot 10^8) 3.14/2 = 3.12 \cdot 10^{-25} [JT^{-1}] \tag{5.3}$$

The primary sources of uncertainty were caused by radius measurements from the images, slight alignment inaccuracies, and the limitations of the magnetic field probe in providing accurate estimates for the magnetic flux density at the location of the Cadmium lamp. Despite these minor sources for random error, the experiment was performed successfully and yielded values close to that expressed in literature, all values falling within statistical uncertainty. In the future, a more accurate method of measuring magnetic field strength could be used to mitigate the systematic error which arose from the calculation of the magnetic field current relationship.

6 Discussion

Looking back on the investigation as a whole, it is clear that the normal Zeeman effect was effectively investigated in a detailed manner. Not only was the transverse Zeeman effect quantitatively observed, through the analysis of the relationship between wavenumber change $\Delta\tilde{\nu}$ against magnetic flux density B, but the longitudinal normal Zeeman effect as well, qualitatively examining the circular polarization resulting from parallel-wise emergent photons in a magnetic field as seen in figure 5. While all results gathered throughout the whole of this investigation are adherent to theoretical expectations to a commensurable degree, considerable improvements to the experimental method could be made. As one can see in table 2 and figure 4, the absolute error of each wavenumber change measurement is quite large in comparison to other errors throughout this report. Looking for possible causes, the most probable is the distortion caused due to the spherical aberration of the biconvex lenses used in the optical setup. Although this was attempted to be mitigated, it was found to be difficult to remove all distortion. When looking through the objective lens at the diffraction grating screen, the patterns appeared slightly oblong, potentially leading to measurements where the ring radii could not as accurately be measured.

In addition to optical distortion due to spherical aberration, a significant error source during the longitudinal Zeeman effect examination was photon attenuation. Since the light emerging along the magnetic field axis is already weaker in intensity, a considerable portion of it failed to reach the detector. This made it difficult to see the circular patterns. Because of this, the diaphragm was removed to allow more light to enter the optical path, which functioned partially. This caused a reduction in the image contrast and increased the human error a bit. Future experiments could be improved from the use of higher sensitivity detectors or better optical alignment to reduce the impact of photon losses.

In support of the theoretical expectations, a clear linear relationship was established between the current through the electromagnets and the resulting magnetic flux density B, expressed as: $B = (0.0585 \pm 0.0007)I + 3.66 \cdot 10^3$. This experiment served as a basis for calculating magnetic field values. Of course, this could be improved at the cost of more time by manually checking the magnetic field strength before each measurement rather than using a trend-line. During the transverse Zeeman effect examination, for a magnetic field strength of $B = 0.4714 \pm 0.0007[T]$, the shift in wavenumber was obtained to be: $\Delta\tilde{\nu} = 48.90 \pm 6.77[m^{-1}]$. This value was derived from measurements of ring displacements at a fixed current of 8A. For that specific current, the average δ was determined to be $\delta_{8A} = 7.50 \pm 0.997[m^2]$ and the mean difference factor $\Delta_{8A} = 25.56 \pm 0.998[m^2]$. The same was done for other currents, and corresponding $\Delta\tilde{\nu}$ values were calculated. By analysing the trend of calculated wavenumber shifts $\Delta\tilde{\nu}$ against magnetic field strength, the slope of the linear fit was found to be $93.55 \pm 3.14[m^{-1}T^{-1}]$. The obtained slope allowed for the calculation of the Bohr magneton, which was obtained to be: $\mu_B = (9.30 \pm 0.31)10^{24}[JT^{-1}]$. While the final result exhibits minor error, its uncertainty allows the value to fall within the expected theoretical value, indicating quality of measurement.

7 Conclusion

The qualitative and quantitative investigation of the normal transverse and longitudinal Zeeman effect yielded very precise results which closely adhered to the theoretical expectations across all areas of measurement and calculation. While some level of error was present throughout some measurements, specifically that of the Bohr magneton, all trends fit the theoretical description to a commensurable degree, and all significant theoretical constants were calculated to an acceptable level of accuracy. To begin the investigation, the relationship between electromagnetic coil current and magnetic flux density was calculated to have a linear relationship consistent with the formula:

$$B = 0.0585(I) + 3.66 \cdot 10^{-3} \tag{7.1}$$

Using this formula to interpolate the fixed current values applied to the Cadmium sample during the calculation of the change in wavenumber $\Delta\tilde{\nu}$ for each current, the relationship between $\Delta\tilde{\nu}$ and the magnetic flux density B was determined to follow the linear equation:

$$\Delta\tilde{\nu} = 93.547B + 4.8988 \tag{7.2}$$

Using this equations slope, and its corresponding uncertainty, the value of the Bohr magneton was consequently calculated via the application of formula 2.7 to a final value of:

$$\mu_B = (9.30 \pm 0.31) \cdot 10^{-24}[JT^{-1}] \tag{7.3}$$

Compared to the theoretical value of the Bohr magneton $\mu_B = 9.274 \cdot 10^{-24}[JT^{-1}]$, the results obtained very closely match with the theoretical value of the constant. Lastly, the circular polarization of parallel aligned emitted electromagnetic waves subject to a magnetic field was verified qualitatively, as successfully indicated in figure 5. For future experiments related to the normal Zeeman effect, the influence of spherical aberration and photon attenuation will be minimized to better the reliability of interference radii measurement. In doing so, an even more insightful and accurate analysis may be conducted, mitigating the present random error, and providing even more reliable values of theoretical constants. Overall, the calculated constant of the Bohr magneton and the observed behavior of the longitudinal Zeeman effect were effectively examined and calculated to a commensurable degree.

References

Fernandez, F., SepÃžlveda, A., Trincavelli, J., & Castellano, G. (2022). L-shell ionization of cd: Structure of the x-ray emission spectrum. *Ultramicroscopy*, *232*, 113401. Retrieved from https://www.sciencedirect.com/science/article/pii/S0304399121001790 doi: https://doi.org/10.1016/j.ultramic.2021.113401

Materny, P. D. A., & Mohaghegh, D. F. (2025). Advanced physics lab ii manual. *Constructor University*.

8 Appendices

8.1 Tables

Measured Ring Radii (mm) and Calculated $\Delta_a, \Delta_b, \delta$ for Current $7[A] \rightsquigarrow 0.413[T]$					
Diff. Order P	r_a $\pm 0.05[mm]$	r_b $\pm 0.05[mm]$	δ	Δ_a	Δ_b
1	4.9	4.2	6.37		
2	6.9	6.3	7.92	23.6	22.05
3	8.6	8.2	6.72		
4	10.1	9.8	5.97	28.05	28.8

Measured Ring Radii (mm) and Calculated $\Delta_a, \Delta_b, \delta$ for Current $6[A] \rightsquigarrow 0.354[T]$					
Diff. Order P	r_a $\pm 0.05[mm]$	r_b $\pm 0.05[mm]$	δ	Δ_a	Δ_b
1	4.9	4.5	3.76		
2	6.9	6.5	5.36	23.6	22
3	8.6	8.3	5.07		
4	9.8	9.5	5.79	22.08	21.36

Measured Ring Radii (mm) and Calculated $\Delta_a, \Delta_b, \delta$ for Current $5[A] \rightsquigarrow 0.296[T]$					
Diff. Order P	r_a $\pm 0.05[mm]$	r_b $\pm 0.05[mm]$	δ	Δ_a	Δ_b
1	4.7	4.3	3.6		
2	7	6.5	6.75	26.91	23.76
3	8.4	8	6.56		
4	9.8	9.6	3.88	25.48	28.16

Measured Ring Radii (mm) and Calculated $\Delta_a, \Delta_b, \delta$ for Current $4[A] \rightsquigarrow 0.238[T]$					
Diff. Order P	r_a $\pm 0.05[mm]$	r_b $\pm 0.05[mm]$	δ	Δ_a	Δ_b
1	4.7	4.2	4.45		
2	6.7	6.4	3.93	22.8	23.32
3	8.5	8.3	3.36		
4	9.9	9.7	3.92	25.76	25.2

Relationship between Current (A) and Magnetic Field Strength (T)	
Current $\pm 0.01[A]$	Magnetic Field Strength $\pm 0.001[T]$
1.10	0.064
1.97	0.116
3.00	0.177
4.33	0.258
5.00	0.299
6.12	0.366
7.11	0.426
8.12	0.485
9.00	0.530
10.07	0.579